Passivity-Based Zero-Sequence LC Resonance Suppression Method for Parallel Inverters System With Modified LCL Filter

Rui Zhang, *Member, IEEE*, Shumei Chi, Xiangyang Xing, *Member, IEEE*, Chenghui Zhang, *Fellow, IEEE*, and Frede Blaabjerg, *Fellow, IEEE*

***Abstract*—Parallel inverters system with modified *LCL* filters may trigger zero-sequence *LC* (ZSLC) resonances. Especially in high-power applications, lower switching frequencies are usually adopted to reduce switching losses. In this situation, conventional inverter-side circulating current feedback (ICCF) control cannot behave as expected and introduces new stability issues due to high control delays. To deal with this situation, a passivity-based ZSLC resonance damping method is proposed. First, the equivalent admittance model of ICCF control is established for the first time, which is decomposed into passive component and active component. The results show that the system stability is determined by the active component and the inverter output admittance ratio. Second, by analyzing the frequency-domain characteristics of active components, it is found that the control delay introduces a negative conductance that affects the stability of the ICCF control. Accordingly, a controllable admittance component is added to correspondingly reshape the inverter output admittance characteristics under high control delay conditions, which can mitigate the detrimental impact of control delay in the active component. Thus, the proposed control strategy can enhance the system stability and the circulating resonance current can be effectively attenuated in high-power applications. Finally, the feasibility and correctness of the proposed scheme are verified by the experiments.**

***Index Terms*—Modeling and analysis, parallel inverters, zero-sequence LC (ZSLC) resonance suppression.**

I. Introduction

GRID-CONNECTED systems are the key interface between renewable energy and the grid, which are widely applied to achieve a flexible and efficient power conversion [1], [2], [3]. Recently, with the increasing installed sustainable energy capacity, the parallel operation scheme of inverters has attracted much attention in high power applications [4], [5]. However, the zero-sequence loops of parallel system inevitably introduce zero-sequence circulating currents problems, which will disturb the output currents and reduce the system stability [6], [7].

Various hardware methods and modulation methods have been reported to cope with the circulating currents. On one hand, many new converter topologies are proposed in [8], [9], and [10]. By adding additional power devices or changing the circuit structure, the zero-sequence loops are blocked to suppress the circulating currents. On the other hand, improved modulation schemes are also often adopted to achieve circulating currents mitigation [11], [12], [13], which achieves the control targets by adjusting the switching sequence of the inverter. However, high losses and degradation of the harmonic attenuation ability are issues that require careful consideration with the above methods [14].

The above drawbacks can be remedied by modified *LCL* (MLCL) filter [15]. By adding a low-impedance path in the capacitive branch, the circulating currents are confined within the inverter system without any additional hardware cost or harmonic increase. Nevertheless, the inclusion of the new zero-sequence loop introduces a risk of additional zero-sequence *LC* (ZSLC) resonances, which may interact with the control loops and have the tendency to destabilize the inverter system.

Continuous research efforts have been devoted to cope with *LCL* resonance, which can be primarily categorized as passive damping [16] and active damping [14], [17], [18], [19], [20], [21]. Among these schemes, the active damping schemes are more acceptable for economic reasons and superior performance, which emulate a virtual damping by feeding back of state variables. However, the adverse impacts of control delay on ZSLC resonance active damping should be carefully considered, which can inevitably change the control characteristics [22]. Especially in high-power parallel system, the switching frequency of the inverter is usually limited to reduce switching losses, resulting in large control delays. In this situation, the active damping may exhibit negative damping characteristics, which will significantly weaken the effectiveness of the ZSLC resonance control and lead to system instability.

Received 20 February 2025; revised 9 July 2025 and 14 August 2025; accepted 16 September 2025. Date of publication 18 September 2025; date of current version 13 November 2025. This work was supported in part by the National Natural Science Foundation of China under Grant 623B2069, Grant 62222309, and Grant 62573256, in part by the Key Research and Development Program of China under Grant 2022YFF0712700, in part by the Shandong Provincial Key Research and Development Program under Grant ZFJH202301, in part by the Major Scientific and Technological Innovation Project of Shandong Province under Grant 2024ZLGX04, and in part by the Postdoctoral Fellowship Program and China Postdoctoral Science Foundation under Grant BX20250396. Recommended for publication by Associate Editor Y. Xue. *(Corresponding author: Xiangyang Xing.)*

Rui Zhang, Shumei Chi, Xiangyang Xing, and Chenghui Zhang are with the School of Control Science and Engineering, Shandong University, Jinan 250061, China (e-mail: sduzr2025@sdu.edu.cn; chishumei@mail.sdu.edu.cn; xyxing@sdu.edu.cn; zchui@sdu.edu.cn).

Frede Blaabjerg is with AAU Energy, Aalborg University, DK-9220 Aalborg, Denmark (e-mail: fbl@et.aau.dk).

Color versions of one or more figures in this article are available at https://doi.org/10.1109/TPEL.2025.3611830.

Digital Object Identifier 10.1109/TPEL.2025.3611830

Existing literature has conducted some research on the impact of control delay on the stability of resonance control [23], [24], [25], [26]. In [23] and [24], the influence of control delay on the filter capacitor voltage feedforward scheme and the grid-side current control is analyzed, and the control delay is reduced through the multi-sampling mode to enhance the control performance. To improve the resonance suppression effect of virtual damping, the influence mechanism of control delay is discussed and a capacitor-current-feedback active damping with reduced computation delay is designed in [25]. In [26], the harmful influence of grid impedance and the control delay on inverter control stability are analyzed and mitigated by a dual-current active damping control strategy. Nevertheless, the above analysis mainly focuses on differential-mode (DM) resonance control strategies. The stability of resonance control is determined by the output admittance and external admittance [16], [27]. For the ZSLC resonance control in the MLCL-type parallel inverters system, the frequency-domain characteristics of the output admittance and external admittance are influenced by the zero-sequence loops between parallel inverters, which differs from DM resonance control and has not been fully studied in the existing literature. Thus, due to the different admittance characteristics, the impact of control delay on the stability of resonance control varies and compromises the performance manifestation of ZSLC resonance control under high delay conditions [28].

To alleviate the ZSLC resonance problem introduced by the MLCL filter, some studies have been carried out in the existing literature [29], [30], [31], [32]. In [29], the ZSLC resonance peak introduced by MLCL filters is effectively suppressed by incorporating inverter-side circulating current feedback (ICCF) control. In [30], ZSLC resonance current in the reduced-switch-count three-level inverters is constrained by regulating the duty cycle of small vectors using a distribution factor and introducing a finite-time controller. In [31] and [32], modified DPWM and current control techniques are applied to achieve efficient ZSLC resonance mitigation. However, the adverse impacts of control delay on ZSLC resonance control are ignored in the above methods to simplify the analysis, which will significantly weaken the control performance and lead to system instability. Recently, as a promising solution to analyze the stability of inverter control and cope with the instability challenge, the frequency-domain passivity theory is introduced into the grid-connected inverter control, which provides an admittance specification to ensure the stability of inverter control [27], [33], [34], [35]. For the grid-side current-controlled *LCL*-type inverter, an impedance model is established and analyzed in [27]. Based on this, an improved capacitor voltage feedforward active damping is proposed to achieve the passive output impedance of the inverter. However, the measurement of the filter capacitor voltage incurs additional costs and complexity, especially in the parallel inverter system. In [33], a PCC voltage feedforward method is proposed to improve the passivity of grid-side DM current control, which can improve the stability of grid-connected inverters with different grid impedances. In [34] and [35], proper phase compensation is introduced into the current control loop and the capacitor current feedback loop to mitigate the impact of fluctuations in grid and filter parameters. These works mainly focus on grid-side current control and resonance control based on DM signal feedback. Nevertheless, additional sensors are inevitable and the DM state variables feedback in above methods cannot enhance the passivity of ZSLC resonance control. Furthermore, compared with grid-side current control, ICCF control is a stronger candidate for circulating resonance current suppression since no additional current sensors are required. In parallel MLCL-type inverter system, due to the distinct coupling paths of ZSLC resonance and DM resonance, their external admittances differ fundamentally. This results in unique resonance frequencies and passivity requirements. In this situation, the intersection points in the amplitude-frequency curves of the inverter output admittance and external admittance are completely different, which leads to the established DM admittance reshaping methods cannot guarantee the passivity for ZSLC resonance control. Therefore, these methods may not work effectively with ICCF control and there is still a lack of a passivity-based control method that ensures the stability of ZSLC resonance control, making it immune to high control delay in high-power applications.

To overcome these limitations, a passivity-based ZSLC resonance damping method is proposed in this article to improve the stability of ICCF control and the suppression performance of circulating resonance current. The main contributions are summarized as follows.

1) In the reported works, existing ZSLC resonance suppression methods fundamentally overlook the destabilizing effect of control delays in the parallel MLCL-type inverter system. To solve this problem, first, an admittance decomposition model of ICCF control is established, which contains a passive component of the filter and an active component of the controller and control delay. Meanwhile, by analyzing the interaction between inverter output admittance and zero-sequence external admittance, the instability range of ICCF control can be accurately identified.
2) Then, the zero-sequence resonance characteristics under different control delays are analyzed. The results indicate that when the control delay increases, the intersection points of the magnitude-frequency curves of the ICCF output admittance and the zero-sequence external admittance may shift into a nonpassive region, which will compromise system stability.
3) Based on the above model and analysis, a passivity-based ZSLC resonance damping method is proposed. By introducing a controllable admittance component, the frequency-domain characteristics of the ICCF control can be correspondingly adjusted under high control delay to optimize the passive region. In this case, the intersection point of the magnitude-frequency curves returns to the stable region. Therefore, the proposed method can maintain stability under external parameters variation or zero-sequence resonance peaks shift, achieving higher disturbance rejection and broader adaptability than conventional methods.

The rest of this article is organized as follows. In Section II, the admittance decomposition zero-sequence model of the ICCF control is established and analyzed in details. In Section III, the effects of control delay on control characteristics and system

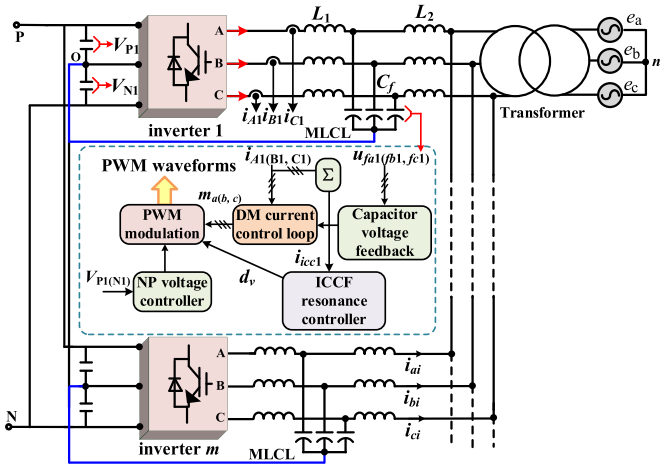

Fig. 1. Topology and control diagram of the parallel inverters with MLCL filters and ICCF control.

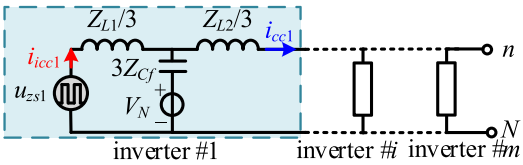

Fig. 2. Zero-sequence model of parallel inverters with MLCL filter.

stability are explained. Based on this, the stability enhancement of the ZSLC resonance controller and the effective suppression of the circulating resonance current are achieved by admittance reshaping. Comparative experimental results are provided in Sections IV. Finally, Section V concludes this article.

II. System Description and Admittance -Based Decomposition Zero-Sequence Model

A. System Description

The control structure and topology of parallel three-level inverters system with MLCL filter are shown in Fig. 1. V_P and V_N are the dc-link capacitor voltages. L_1 and L_2 are the inverter-side inductor and the grid-side inductor. C_f is the filter capacitor. By adding a low-impedance zero-sequence loop between the neutral point of the dc-link and the common point of the filter capacitor, MLCL filter can suppress the circulating currents without any additional cost and power loss. Meanwhile, by controlling the inverter-side circulating currents, the ICCF control is applied to solve the ZSLC resonance problem that may be caused by the MLCL filter.

B. Modeling of ICCF Control

Based on the circuit configuration in Fig. 1, the zero-sequence model of parallel inverters with MLCL filter is shown in Fig. 2, where $u_{zsi} = u_{AOi} + u_{BOi} + u_{COi}$ $(i = 1, 2, \ldots m)$ is the zero-sequence excitation source of the ith inverter; $i_{cci} = i_{ai} + i_{bi} + i_{ci}$ is the grid-side circulating current of the ith inverter; $i_{icci} = i_{Ai} + i_{Bi} + i_{Ci}$ is the inverter-side circulating current

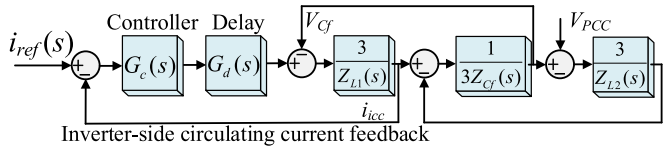

Fig. 3. Block diagram of ICCF control.

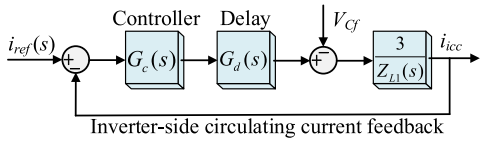

Fig. 4. Simplified block diagram of ICCF control.

of the ith inverter; Z_{L1}, Z_{L2} and Z_{Cf} are the impedances of filter inductors and filter capacitor. Since parallel inverters are typically connected to the grid via transformers, the transformer blocks the circulating current path. Therefore, the circulating resonance currents circulate exclusively through MLCL filters and between inverters, achieving decoupling from network impedance.

The ICCF control structure can be represented by the block diagram in Fig. 3. G_c(s) is a proportional-integral controller, and its transfer function is expressed in (1). G_d(s) represents the control delay, which includes computation delay and PWM delay. For computation delay, when the counter reaches zero and/or the period value, the duty-ratio is updated to the comparison register and it will introduce a delay of one period in the control loop. For PWM delay, the duty-ratio signal remains constant within the sampling period, which has the characteristics of a zero-order holder and introduces a delay of 1/2 period. Therefore, the model for the control delay G_d can be obtained as (2)

$$G_c(s) = K_p + \frac{K_i}{s} \tag{1}$$

$$G_d(s) = e^{-3sT_s/2} \tag{2}$$

where K_p and K_i are control parameters and T_s is the switching period.

The controlled plant for the inverter-side circulating current control loop is the filter inductor L_1. The filter capacitor C_f and the grid-side inductance L_2 can be regarded as the external impedance. In this case, the model shown in Fig. 3 can be simplified to Fig. 4. Accordingly, the loop gain and closed-loop response of the ICCF control loop are obtained as

$$G_{op}(s) = \frac{3G_c(s) \cdot G_d(s)}{Z_{L1}(s)} \tag{3}$$

$$i_{icc}(s) = \frac{G_{op}(s)}{1 + G_{op}(s)} i_{\text{ref}}(s) - V_{Cf}(s) Y_{iod}(s) \tag{4}$$

where V_{Cf}(s) is the filter capacitor voltage and Y_{iod}(s) is the inverter output admittance, which is expressed as

$$Y_{iod}(s) = \frac{i_{icc}}{V_{Cf}} = \frac{3}{Z_{L1}(s)[1 + G_{op}(s)]}. \tag{5}$$

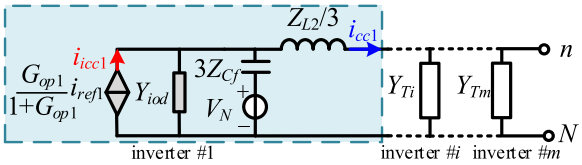

Fig. 5. Norton equivalent zero-sequence model of parallel inverters with MLCL filter.

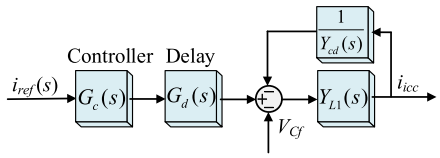

Fig. 6. Equivalent block diagram of ICCF control.

Then, the zero-sequence model of the parallel inverters system can be simplified as the Norton equivalent circuit, as shown in Fig. 5.

Based on the Norton equivalent model, the filter capacitor voltage and the inverter-side circulating current can be further derived as

$$V_{Cf}(s)=\frac{3[Z_{L2}(s)Y_f(s)+3]\cdot Z_{Cf}(s)i_{icm}(s)}{Z_{L2}(s)Y_f(s)+9Z_{Cf}(s)Y_f(s)+3} \tag{6}$$

$$i_{icc}(s)=\frac{1}{1+Y_{iod}(s)/Y_T(s)}\frac{G_{op}(s)}{1+G_{op}(s)}i_{ref}(s) \tag{7}$$

where $Y_f(s)=(C_fL_1s^2+1)/(L_1L_2C_fs^3+L_1s+L_2s)$ is the equivalent admittance of the filter; $Y_T(s)=3[Z_{L2}(s)Y_f(s)+3]mZ_{cf}(s)/[Z_{L2}(s)Y_f(s)+9Z_{cf}(s)Y_f(s)+3]$ is the external equivalent admittance of the parallel inverters excluding the first inverter.

It is seen from (7) that the characteristics of the ICCF control loop are affected by the closed-loop gain and the admittance ratio $Y_{iod}(s)/Y_T(s)$. For closed-loop gain, appropriate parameter design can ensure stable control. Therefore, the stability of the system is mainly determined by the admittances $Y_{iod}(s)$ and $Y_T(s)$, which form a minor feedback loop. In order to satisfy the Nyquist stability criterion, the phase margin at the intersection of the amplitude-frequency response curves of $Y_{iod}(s)$ and $Y_T(s)$ must be greater than 0°. Consequently, the stability condition of the system can be expressed as

$$PM=180^\circ-[\angle Y_{iod}(s)-\angle Y_T(s)]>0^\circ. \tag{8}$$

Further, in order to facilitate the analysis of the frequency domain characteristics of $Y_{iod}(s)$, substituting (3) to (5), $Y_{iod}(s)$ is further derived as

$$Y_{iod}(s)=\frac{1}{\underbrace{1/Y_{L1}(s)}_{\text{passivecomponents}}+\underbrace{1/Y_{cd}(s)}_{\text{active components}}} \tag{9}$$

where $Y_{L1}(s)=3/Z_{L1}(s)$, $Y_{cd}(s)=1/G_c(s)G_d(s)$.

Accordingly, the ICCF control block diagram can be equivalent to Fig. 6. It is seen that the output admittance of the inverter is composed of passive component $Y_{L1}(s)$ and active component $Y_{cd}(s)$ in series. The passive component is determined by passive filter and the active component is determined by controller and control delay. Thus, the influence of different factors on the output admittance characteristics can be discussed separately.

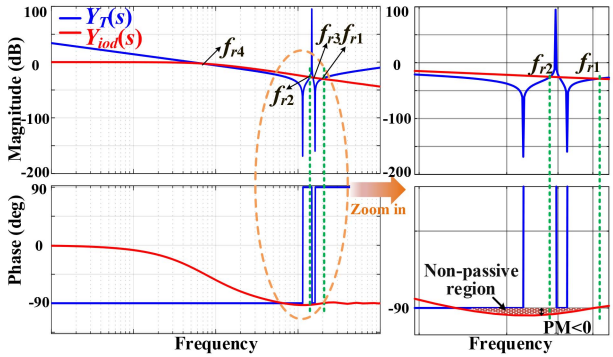

Fig. 7. Bode diagrams of $Y_{iod}(s)$ and $Y_T(s)$.

III. Control Delay Analysis and Proposed ZSLC Resonance Suppression Strategy Design

A. Impact of Control Delay on System Stability

Based on the model analysis in the Section II, the stability of ICCF control is determined by the phase characteristics of $Y_{iod}(s)$ and $Y_T(s)$. Fig. 7 shows the bode diagrams of $Y_{iod}(s)$ and $Y_T(s)$. It is seen that the phase of $Y_T(s)$ is between $-90°$ and 90°. According to the passivity theory [16], [24], the control stability is mainly affected by the nonpassive region of inverter output admittance $Y_{iod}(s)$. Specifically, there are four amplitude-frequency response intersection points ($f_{r1}\sim f_{r4}$) in Fig. 7. Among them, the phase of $Y_T(s)$ at f_{r3} and f_{r4} is $-90°$. Therefore, only the phase margin at f_{r1} and f_{r2} may be less than 0°, which should be taken into primary consideration. f_{r1} and f_{r2} are expressed as

$$f_{r1}=\frac{1}{2\pi}\sqrt{\frac{L_1+L_2}{L_1L_2C_f}} \tag{10}$$

$$f_{r2}=\frac{1}{2\pi}\sqrt{\frac{1}{L_1C_f}}. \tag{11}$$

If the amplitude-frequency response intersection points f_{r1} and f_{r2} are in the nonpassive region as shown in Fig. 7, the control system will be unstable. Therefore, the phase of $Y_{iod}(s)$ at the intersection point should be within $[-90°, 90°]$ to avoid ZSLC resonance. Based on this, the stability condition for the ICCF control can be further intuitively represented as requiring the real part of the inverter output admittance at the intersection point to be greater than zero [16], which can be expressed as

$$\mathrm{Re}[Y_{iod}(j\omega)]\,|_{f_{r1},f_{r2}}\geq 0. \tag{12}$$

According to (9), the real part of passive component $Y_{L1}(s)$ is zero. Thus, the real part of the inverter output admittance $Y_{iod}(s)$ is determined by the active component $Y_{cd}(s)$. Furthermore, the integral term of the PI controller can be designed to have

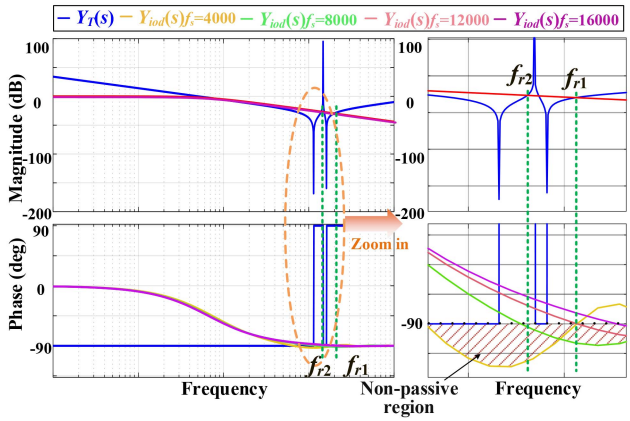

Fig. 8. Bode diagrams of $Y_{iod}(s)$ and $Y_T(s)$ with different f_s.

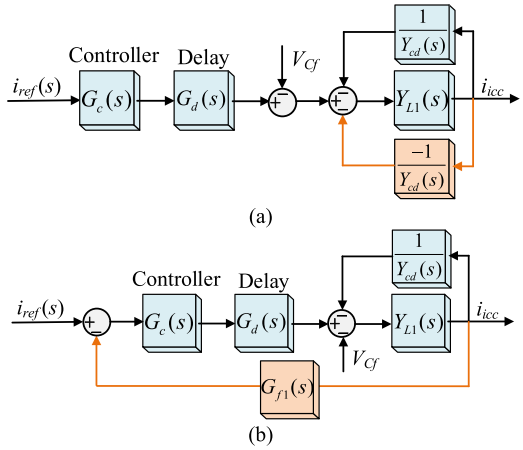

Fig. 9. ZSLC resonance control block based on the admittance reshaping. (a) Modified model. (b) Simplified model.

a negligible influence on the system stability. In this situation, $Y_{cd}(s)$ is expressed as

$$Y_{cd}(s) \approx \frac{1}{K_p G_d(s)}. \tag{13}$$

Based on Euler's formula, $Y_{cd}(s)$ can be equivalent to the parallel form of equivalent conductance G_{eq} and susceptance B_{eq}, which is expressed as

$$\begin{aligned} Y_{cd}(s=j\omega) &= e^{3j\omega T_s/2}/K_p \\ &= \underbrace{\cos(3\omega T_s/2)/K_p}_{G_{\text{eq}}} + \underbrace{j\sin(3\omega T_s/2)/K_p}_{B_{\text{eq}}}. \end{aligned} \tag{14}$$

It is seen that due to the existence of the delay link, the active damping characteristic changes from an equivalent conductance to an equivalent admittance. More importantly, the amplitude of the equivalent conductance becomes negative as the frequency changes, that is, the real parts of Y_{iod} and Y_{cd} may be negative, which is expressed as

$$\text{Re}[Y_{iod}(s=j\omega)] = \text{Re}[Y_{cd}(s=j\omega)] = \cos(3\omega T_s/2)/K_p. \tag{15}$$

Obviously, the real part of the $Y_{iod}(s)$ is affected by the switching period T_s. Between $f_s/6$ to $f_s/2$, the real part and the output conductance is negative, which indicates that there is a nonpassive region. The theory analysis is consistent with Fig. 7. Generally, the intersection point of the amplitude-frequency response curves of $Y_{iod}(s)$ and $Y_T(s)$ is fixed. Therefore, the stability of the system is determined by the nonpassive region. Fig. 8 shows the bode diagrams of $Y_{iod}(s)$ and $Y_T(s)$ with different switching frequencies. It can be observed that when the switching frequency is high, both f_{r1} and f_{r2} are in the passive region and the phase margin is greater than 0°. At this point, the control system is stable. However, as the switching frequency decreases, the frequency range of the nonpassive region gradually decreases. It may become a nonpassive region at f_{r1} and f_{r2}, which causes control instability and deterioration of ZSLC resonance. Thus, the passivity of the traditional ICCF control with low switching frequency needs to be further improved.

B. Proposed ZSLC Resonance Suppression Strategy

Based on the above stability analysis, the existence of a nonpassive region in the inverter output admittance $Y_{iod}(s)$ will cause control instability. Therefore, the passivity and stability of the system are improved by reshaping the output admittance in this article.

Specifically, the nonpassive region of $Y_{iod}(s)$ is mainly determined by the active component $Y_{cd}(s)$. Accordingly, by changing $Y_{cd}(s)$, the inverter output admittance can be reshaped and the nonpassive region can be reduced. To cancel out the active component, as shown in Fig. 9(a), an ICCF path is added to the control loop and the feedback gain is set to $-1/Y_{cd}(s)$. In this way, a negative series virtual admittance is introduced, which can improve the control stability by reducing the nonpassive region of $Y_{cd}(s)$.

In order to make the control loop applicable in practice, the feedback points of i_{icc} are moved forward to the input of the controller, as shown in Fig. 9(b). At this time, the gain of the added feedback path can be obtained as

$$G_{f1}(s) = \frac{-1/Y_{cd}(s)}{G_c(s)G_d(s)} = \frac{-G_c(s)G_d(s)}{G_c(s)G_d(s)} = -1. \tag{16}$$

It is seen from Fig. 9(b), the increased feedback path is the positive feedback of i_{icc}. In this case, although the virtual admittance can reduce the nonpassive region, the positive feedback will change the phase margin of the system and reduce the low-frequency loop gain. To overcome this limitation, a high-pass filter is adopted in the feedback loop and merged with the original feedback loop as shown in Fig. 10. The feedback gain can be obtained as

$$G_{f2}(s) = \frac{1}{1+\delta s} \tag{17}$$

where $\delta = 1/\omega_c$ is control coefficient; ω_c is cut-off frequency.

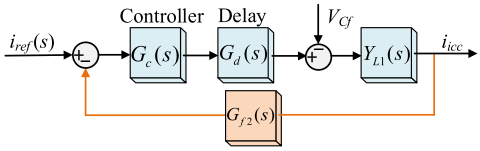

Fig. 10. Equivalent model of the improved zero-sequence control block with admittance reshaping and high-pass filter.

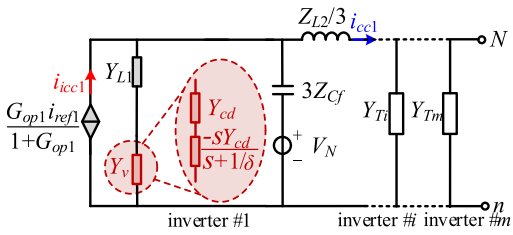

Fig. 11. Reshaped admittance model of parallel inverters with MLCL filter.

Based on this, the introduced virtual admittance and the reshaped inverter output admittance are obtained as

$$Y_v(s) = \frac{Y_{cd}(s)}{G_{f2}(s)} = \frac{1+\delta s}{K_p e^{-3sT_s/2}} \tag{18}$$

$$Y_{iod1}(s) = \frac{1}{1/Y_{L1}(s) + 1/Y_v(s)}. \tag{19}$$

Then, the admittance model of the parallel inverters system with MLCL filters can be further modified as Fig. 11. It is seen that in addition to passive component $Y_{L1}(s)$ and active component $Y_{cd}(s)$, controllable components are added to the reshaped output admittance. Therefore, by adjusting the introduced virtual admittance, the frequency domain characteristics of the output admittance can be changed to improve the system stability.

Similarly, the real part of the inverter output admittance is determined by $Y_v(s)$, which is expressed as

$$\begin{aligned}\mathrm{Re}[Y_{iod1}(s=j\omega)] &= \mathrm{Re}[Y_v(s=j\omega)] \\ &= [\cos(3\omega T_s/2) - \omega\delta\sin(3\omega T_s/2)]/K_p.\end{aligned} \tag{20}$$

As shown in (20), the real part of the reshaped output admittance $Y_{iod1}(s)$ is affected by the control coefficient δ. Fig. 12 shows the real part curves of the output admittance with different δ. Define the intersection point of the real part curve and 0 as the critical frequency f_c, which is the highest frequency of the nonpassive region. As δ increases, the nonpassive region and f_c gradually shift to lower frequencies. Therefore, the nonpassive region of the system can be adjusted by changing δ. To maintain control stability, the phase margin of the amplitude-frequency response intersection f_{r1} and f_{r2} must exceed 0°—equivalently, the real part of the output admittance $Y_{iod}(s)$ must be greater than 0. It is seen from Fig. 12 that to ensure the real part of $Y_{iod}(s)$ remains positive, the critical frequency f_c must be less than both f_{r1} and f_{r2}.To meet the above requirements, the control

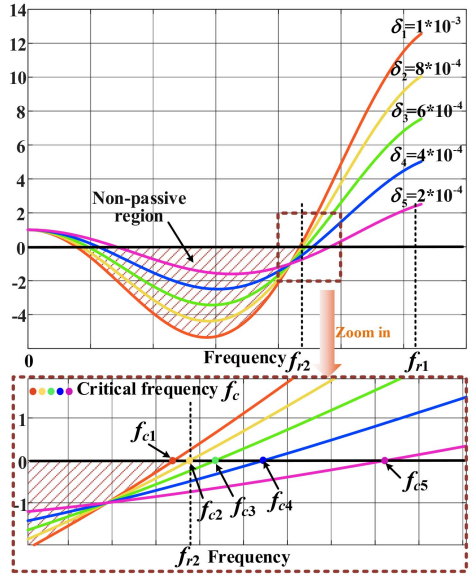

Fig. 12. Real part curves of the output admittance with different δ.

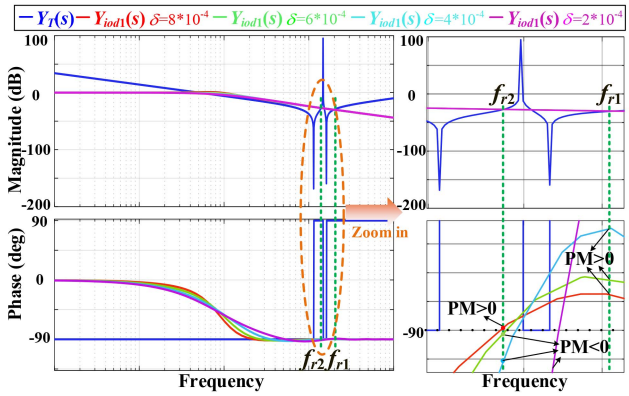

Fig. 13. Bode diagrams of $Y_{iod1}(s)$ and $Y_T(s)$ with different δ.

coefficient δ is obtained as

$$\delta > \frac{\cos(3\pi f_{r2}T_s)}{2\pi f_{r2}\sin(3\pi f_{r2}T_s)}. \tag{21}$$

In order to verify the influence of the control coefficient δ on the output admittance and system stability, a bode diagram of the reshaped output admittance $Y_{iod1}(s)$ with different δ is shown in Fig. 13. It is seen that when the virtual admittance is added, the phase margin of $Y_{iod1}(s)$ and $Y_T(s)$ at the intersection frequency in the magnitude plot gradually increases. When $\delta = 8*10^{-4}$, f_{r1} and f_{r2} are both greater than the critical frequency f_c and the phase margin is greater than zero. Therefore, according to the aforementioned theoretical analysis, the ICCF control in high power applications regains stability.

C. Controller Parameters Design

According to Fig. 10, the open-loop transfer function of the reshaped ICCF control is obtained as

$$G_{op}(s) = G_c(s) \cdot G_d(s) \cdot Y_{L1}(s) \cdot G_{f2}(s) = \frac{3K_P \cdot e^{-3sT_s/2}(\tau_i s + 1)}{\delta \tau_i L_1 s^3 + \tau_i L_1 s^2} \tag{22}$$

where the transfer function $G_c(s)$ of the PI controller is rewritten as a zero-pole form to simplify the analysis

$$G_c(s) = K_p + \frac{K_i}{s} = \frac{K_p(\tau_i s + 1)}{\tau_i s}. \tag{23}$$

Generally, control delay $3T_s/2$ is small enough so that the delay link is approximated as $G_d(s) = 1/(3sT_s/2+1)$ and the $G_{op}(s)$ can be simplified as

$$G_{op}(s) = \frac{3K_P(\tau_i s + 1)}{3T_s\delta\tau_i L_1 s^4/2 + (\delta\tau_i L_1 + 3T_s\tau_i L_1/2)s^3 + \tau_i L_1 s^2}. \tag{24}$$

At the cut-off angular frequency ω_c, the magnitude of open-loop transfer function is 1. Meanwhile, the cut-off angular frequency ω_c is expressed as $2\pi f_s/5$ according to the design rules of control system engineering. Thus, (24) is expressed as

$$A_{op}(\omega_c) = \frac{3K_P\sqrt{(2\tau_i\pi f_s/5)^2 + 1}}{\tau_i L_1 (2\pi f_s/5)^2 \sqrt{[(3\pi/5)^2 + 1][(2\delta\pi f_s/5)^2 + 1]}} = 1. \tag{25}$$

Accordingly, the controller parameters are derived as

$$K_P = \frac{\tau_i L_1 (2\pi f_s/5)^2 \sqrt{[(3\pi/5)^2 + 1][(2\delta\pi f_s/5)^2 + 1]}}{3\sqrt{(2\tau_i\pi f_s/5)^2 + 1}}. \tag{26}$$

Furthermore, when a PI controller is applied, the corner frequency f_L is expressed as

$$f_L = \frac{1}{2\pi\tau_i}. \tag{27}$$

To ensure the response speed of the control system, f_L is designed as

$$f_L = \frac{f_s}{10}. \tag{28}$$

Based on (27) and (28), the controller parameters τ_i can be derived as

$$\tau_i = \frac{n}{2\pi f_L} = \frac{5}{\pi f_s}. \tag{29}$$

IV. Experimental Results

In order to verify the correctness of the theoretical analysis and the effectiveness of the proposed scheme, experimental results are presented. The experiments are performed on a parallel T-type three-level inverter system, which is shown in Fig. 14. The control scheme is implemented with dSPACE DS1005 digital control system. The dc voltage is supplied by dc source and the parallel inverters share the same dc-link voltage. The experimental parameters are given in Table I.

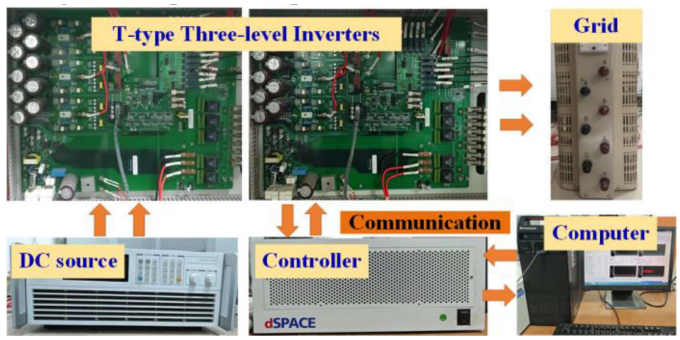

Fig. 14. Experimental platform of parallel T-type three-level inverters.

TABLE I
Experimental Parameters

Parameters	Values
AC grid voltage (e_{abc})	110 Vrms
Reference current (i_{ref1} and i_{ref2})	10 A, 20 A
DC bus voltage (V_{dc1} and V_{dc2})	350 V
DC-link capacitors (C_1, C_2)	3300 μF
Inverter-side inductance (L_1)	2.7 mH
Grid-side inductance (L_2)	1.5 mH
Filter capacitance (C_f)	4.7 μF
Parameters of PI controller (K_p, τ_i)	35.78, 3.98 × 10^{-4}
Control coefficient (δ)	8 × 10^{-4}
IGBT	10-FZ12NMA080SH01-M260F
Current sensor module	VAC4646X400
Voltage sensor module	VSM025A
DC power supply	Chroma 62150H-1000S

The MLCL filters will cause resonance risks when applied to suppress circulating currents. Fig. 15 presents the experimental waveforms of the grid-side currents (i_{a1}, i_{a2}), grid-side circulating current (i_{cc}), inverter-side circulating current (i_{icc1}), and the spectrum of i_{a1} with ICCF control and without circulating resonance current control. When resonance control is not applied in Fig. 15(a), the additional zero-sequence loop triggers ZSLC resonance, which causes the inverter output current to oscillate and the circulating current to increase. Meanwhile, it is seen from the current spectrum that the grid-side current harmonic component is mainly concentrated in the ZSLC resonance peak f_{r1}, which is consistent with the theoretical analysis. In order to improve power quality, conventional ICCF control is usually adopted to suppress the circulating resonance current. As shown in Fig. 15(b), the circulating current can be suppressed and current distortion reduced.

However, the stability of ICCF control needs to be carefully considered in parallel systems. Since the control delay will change the phase-frequency characteristics of the inverter output admittance, the intersection point of the amplitude-frequency curve of the output admittance and the system equivalent admittance may be in the nonpassive region. In this situation, the

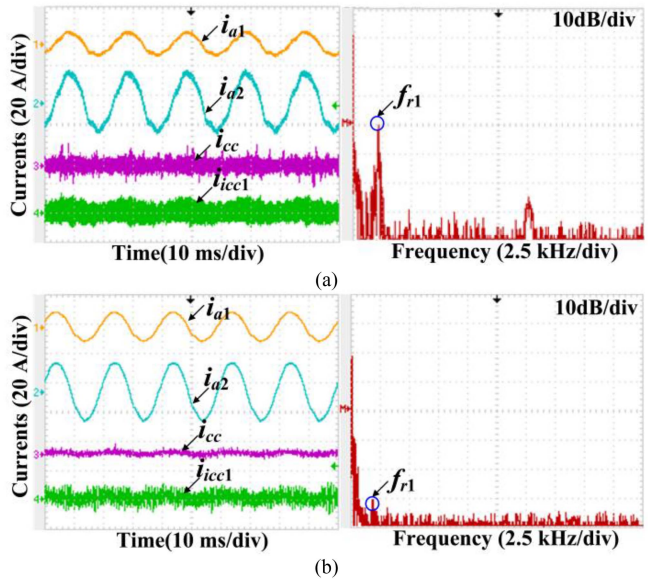

Fig. 15. Experimental waveforms of output currents and the spectrum of i_{a1} ($f_s = 15$ kHz). (a) Without zero-sequence control. (b) ICCF control.

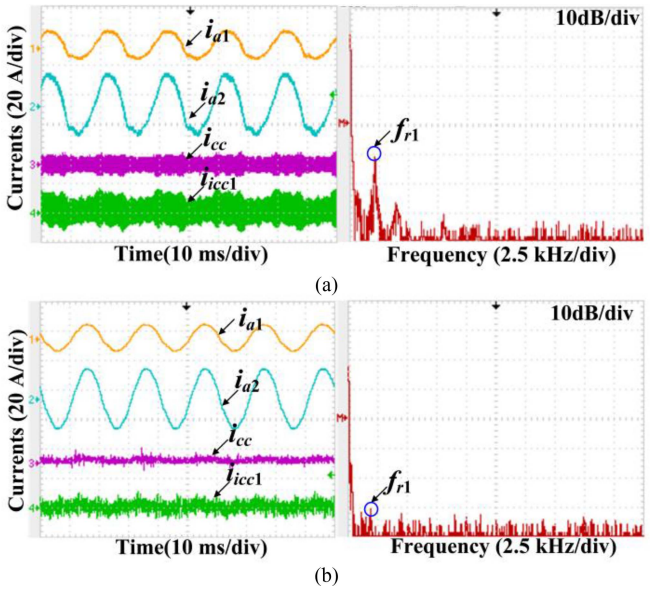

Fig. 16. Experimental waveforms of output currents and the spectrum of i_{a1} with high control delay ($f_s = 4$ kHz). (a) ICCF control. (b) Proposed scheme.

ICCF control cannot effectively suppress the ZSLC resonance as expected. As shown in Fig. 16(a), when the switching frequency is reduced to 4 kHz, the circulating currents in the inverter-side and the grid-side are large. The grid-connected current oscillates violently and the harmonic component at the ZSLC resonance peak increases greatly, which indicates that the ICCF control fails and affects the system stability. When the proposed scheme is applied, by reshaping the inverter output admittance, the system instability point will be relocated to the passive region. Thus, the proposed method can maintain ZSLC resonance suppression performance and the system stability under high control delays without any additional sensors. It is seen from Fig. 16(b) that the

TABLE II
CIRCULATING CURRENTS AND THD OF GRID-SIDE CURRENTS WITH DIFFERENT METHODS

Parameters	ICCF control	Proposed scheme
Grid-side circulating current (i_{cc})	6.8 A	3.1 A
Inverter-side circulating current (i_{icc})	14.1 A	7.7 A
THD of i_{a1}	13.02%	4.39%
THD of i_{a2}	12.81%	3.80%

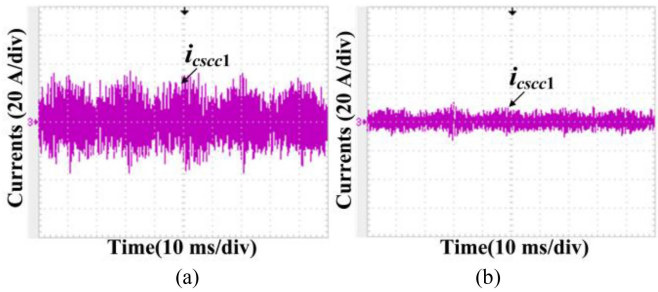

Fig. 17. Experimental waveforms of filter capacitor-side circulating currents with high control delay ($f_s = 4$ kHz). (a) ICCF control. (b) Proposed scheme.

current harmonics at the ZSLC resonance peak are effectively suppressed by the proposed method. The power quality of the output currents is greatly improved.

The amplitude of circulating currents and THD of grid-side currents with different methods are summarized in Table II. It can be seen that compared with ICCF control, the grid-side circulating current and the inverter-side circulating current of the proposed scheme are significantly reduced (about 50%). Meanwhile, the distortion of grid currents is effectively alleviated and THD is reduced.

The filter capacitor-side circulating currents with different methods are shown in Fig. 17. When the ICCF control is applied, the filter capacitor-side circulating current has a large amplitude as seen in Fig. 17(a) (about 32 A) due to the high control delay causing system instability. However, when the proposed method is implemented in Fig. 17(b), the ZSLC resonance can be effectively suppressed and the circulating current on the filter capacitor side is reduced to 10 A.

Fig. 18 illustrates comparative results of the inverter-side currents and current spectrum with different control methods. It is seen that under high control delay, the inverter-side circulating current cannot be effectively suppressed by the ICCF control. In this situation, the inverter-side current oscillates drastically and the harmonic content is mainly concentrated at f_{r1} and f_{r2} as shown in Fig. 18(b). When switching to the proposed method, the amplitude of the circulating current is effectively mitigated. Consequently, the harmonic components of the current are significantly reduced, and the power quality is improved.

To verify the effectiveness of the proposed control parameter design scheme, the transient response of the proposed method is shown in Fig. 19 when the control coefficient δ changes. When δ is set to $1*10^{-3}$, the inverter output current maintains a good power quality. However, when δ is reduced to $6*10^{-4}$, the real

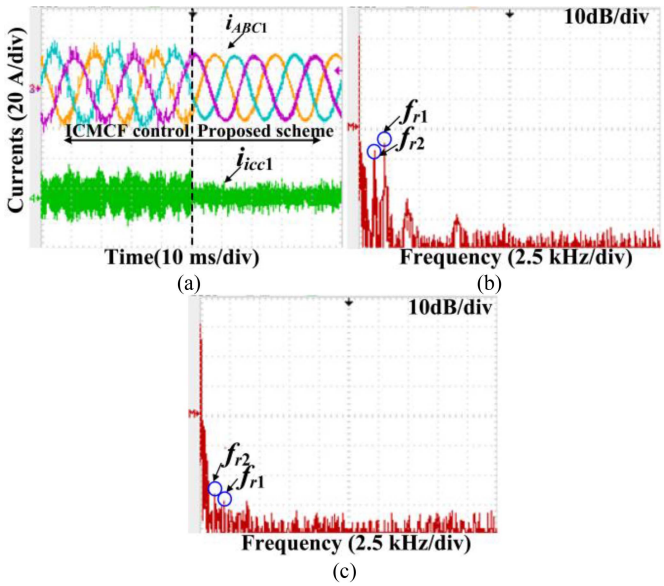

Fig. 18. Dynamic experimental waveforms of inverter-side currents and the spectrum of i_{A1} with high control delay ($f_s = 4$ kHz). (a) Inverter-side currents and circulating current. (b) Spectrum of i_{A1} with ICCF control. (c) Spectrum of i_{A1} with proposed scheme.

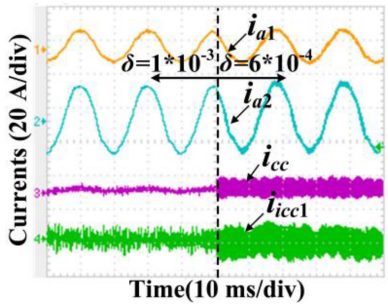

Fig. 19. Dynamic experimental waveforms of output currents with different control coefficients δ ($f_s = 4$ kHz).

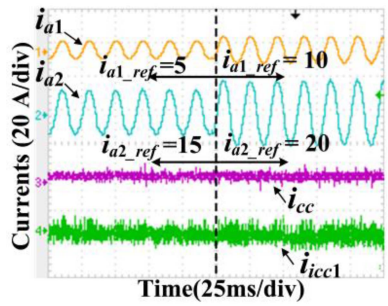

Fig. 20. Dynamic experimental waveforms of output currents with different reference currents ($f_s = 4$ kHz).

part of the reshaped output admittance at f_{r2} is negative. Therefore, the circulating current cannot be effectively suppressed and the output current is severely disturbed, which is consistent with the theoretical analysis.

The current transient responses with different current references are presented in Fig. 20 to further validate the dynamic performance and stability of the proposed method. It can be observed that when the current reference changes, the circulating resonance current can still be effectively controlled. Meanwhile, the quality of the inverter output current can be guaranteed.

V. Conclusion

An improved ZSLC resonance suppression method based on passivity theory is proposed in this article. First, by establishing and analyzing the admittance decomposition zero-sequence model of ICCF control, the influence of control delay on the ZSLC resonance control stability is revealed. Meanwhile, the relationship between the nonpassive region and the admittance ratio is obtained. Based on this, the proposed method changes the nonpassive region by connecting a virtual admittance in series. Without additional sensors, the adverse effects of control delay can be mitigated and the control stability can be enhanced. Furthermore, the effectiveness of the proposed control coefficient design scheme is also verified by experimental results. Compared with the conventional ICCF control, the proposed method can effectively reduce the circulating resonance current (about 50%), and the current ripple is significantly alleviated under high control delay.

References

[1] Y. Yang et al., "A novel continuous control set model predictive control for LC-filtered three-phase four-wire three-level voltage-source inverter," *IEEE Trans. Power Electron.*, vol. 38, no. 4, pp. 4572–4584, Apr. 2023.

[2] X. Guo, Y. Yang, B. Wang, and F. Blaabjerg, "Leakage current reduction of three-phase Z-source three-level four-leg inverter for transformerless PV system," *IEEE Trans. Power Electron.*, vol. 34, no. 7, pp. 6299–6308, Jul. 2019.

[3] P. Shan, Y. Sun, Y. Song, F. Zhang, Y. Li, and K. Sun, "Adaptive parameter tuning and virtual impedance injection control for coupled harmonic mitigation of photovoltaic converter," *IEEE Trans. Power Electron.*, vol. 40, no. 1, pp. 162–175, Jan. 2025.

[4] L. Zhang, K. Sun, Y. Xing, and J. Zhao, "Parallel operation of modular single-phase transformerless grid-tied PV inverters with common DC bus and AC bus," *IEEE J. Emerg. Sel. Topics Power Electron.*, vol. 3, no. 4, pp. 858–869, Dec. 2015.

[5] Q. Qian, S. Xie, L. Huang, J. Xu, Z. Zhang, and B. Zhang, "Harmonic suppression and stability enhancement for parallel multiple grid-connected inverters based on passive inverter output impedance," *IEEE Trans. Ind. Electron.*, vol. 64, no. 9, pp. 7587–7598, Sep. 2017.

[6] K. Sun, X. Lin, Y. Li, Y. Gao, and L. Zhang, "Improved modulation mechanism of parallel-operated T-type three-level PWM rectifiers for neutral-point potential balancing and circulating current suppression," *IEEE Trans. Power Electron.*, vol. 33, no. 9, pp. 7466–7479, Sep. 2018.

[7] C. Du, W. Cai, L. Zhao, Z. Chen, B. Chen, and F. Gao, "Improved finite-time control for circulating current suppression of multiparalleled rectifiers," *IEEE J. Emerg. Sel. Topics Power Electron.*, vol. 11, no. 3, pp. 2767–2779, Jun. 2023.

[8] N. Kumar, M. Mohamadi, and S. K. Mazumder, "Passive damping optimization of the integrated-magnetics-based differential-mode Ćuk rectifier," *IEEE Trans. Power Electron.*, vol. 35, no. 10, pp. 10008–10012, Oct. 2020.

[9] X. Li, Y. Liu, J. Yang, and X. Wu, "Decoupled magnetic integration of symmetrical LCL filter with a common-mode inductor for single-phase grid-connected converters," *IEEE J. Emerg. Sel. Topics Ind. Electron.*, vol. 3, no. 4, pp. 966–977, Oct. 2022.

[10] Y. Yang et al., "A novel cascaded repetitive controller of an LC-filtered H6 voltage-source inverter," *IEEE J. Emerg. Sel. Topics Power Electron.*, vol. 11, no. 1, pp. 556–566, Feb. 2023.

[11] B. Ren, X. Sun, M. Yu, J. Liu, and Q. Zhang, "Circulating current analysis and the improved D–Σ digital control strategy for multiparalleled three-level t-type grid-connected inverters," *IEEE Trans. Ind. Electron.*, vol. 67, no. 4, pp. 2810–2821, Apr. 2020.

[12] T. Xu, F. Gao, K. Zhou, P. Tan, C. Zhang, and E. Chi, "A min–max closed-loop PLL-GSPWM for circulating leakage currents attenuation in PV station," *IEEE Trans. Power Electron.*, vol. 36, no. 9, pp. 10224–10238, Sep. 2021.
[13] P. Zhang et al., "Integration modulation for current ripple and high-frequency zero-sequence circulating current reduction on two-parallel three-level converters," *IEEE Trans. Ind. Electron.*, vol. 71, no. 8, pp. 8216–8226, Aug. 2024.
[14] S. Yang, Z. Yin, C. Tong, Y. Sui, and P. Zheng, "Active damping current control for current-source inverter-based PMSM drives," *IEEE Trans. Ind. Electron.*, vol. 70, no. 4, pp. 3549–3560, Apr. 2023.
[15] J. C. Giacomini, L. Michels, M. C. Cavalcanti, and C. Rech, "Modified discontinuous PWM strategy for three-phase grid-connected PV inverters with hybrid active–passive damping scheme," *IEEE Trans. Power Electron.*, vol. 35, no. 8, pp. 8063–8073, Aug. 2020.
[16] G. Ma, C. Xie, C. Li, J. Zou, and J. M. Guerrero, "Passivity-based design of passive damping for LCL-type grid-connected inverters to achieve full-frequency passive output admittance," *IEEE Trans. Power Electron.*, vol. 38, no. 12, pp. 16048–16060, Dec. 2023.
[17] X. Wang, F. Blaabjerg, and P. C. Loh, "Grid-current-feedback active damping for LCL resonance in grid-connected voltage-source converters," *IEEE Trans. Power Electron.*, vol. 31, no. 1, pp. 213–223, Jan. 2016.
[18] L. Zhou et al., "Inverter-current-feedback resonance suppression method for LCL-type DG system to reduce resonance-frequency offset and grid-inductance effect," *IEEE Trans. Ind. Electron.*, vol. 65, no. 9, pp. 7036–7048, Sep. 2018.
[19] X. Li, J. Fang, Y. Tang, and X. Wu, "Robust design of LCL filters for single-current-loop-controlled grid-connected power converters with unit PCC voltage feedforward," *IEEE J. Emerg. Sel. Topics Power Electron.*, vol. 6, no. 1, pp. 54–72, Mar. 2018.
[20] M. T. Faiz et al., "Capacitor voltage damping based on parallel feedforward compensation method for LCL-filter grid-connected inverter," *IEEE Trans. Ind. Appl.*, vol. 56, no. 1, pp. 837–849, Jan./Feb. 2020.
[21] M. A. Azghandi, S. M. Barakati, and A. Yazdani, "Passivity-based design of a fractional-order virtual capacitor for active damping of multiparalleled grid-connected current-source inverters," *IEEE Trans. Power Electron.*, vol. 37, no. 7, pp. 7809–7818, Jul. 2022.
[22] M. A. Azghandi, S. M. Barakati, and A. Yazdani, "Impedance-based stability analysis and design of a fractional-order active damper for grid-connected current-source inverters," *IEEE Trans. Sustain. Energy*, vol. 12, no. 1, pp. 599–611, Jan. 2021.
[23] S. He, D. Zhou, X. Wang, and F. Blaabjerg, "Passivity-based multisampled converter-side current control of LCL-filtered VSCs," *IEEE Trans. Power Electron.*, vol. 37, no. 11, pp. 13848–13860, Nov. 2022.
[24] X. Zhang, P. Chen, C. Yu, F. Li, H. T. Do, and R. Cao, "Study of a current control strategy based on multisampling for high-power grid-connected inverters with an LCL filter," *IEEE Trans. Power Electron.*, vol. 32, no. 7, pp. 5023–5034, Jul. 2017.
[25] D. Pan, X. Ruan, C. Bao, W. Li, and X. Wang, "Capacitor-current-feedback active damping with reduced computation delay for improving robustness of LCL-type grid-connected inverter," *IEEE Trans. Power Electron.*, vol. 29, no. 7, pp. 3414–3427, Jul. 2014.
[26] Y. Guan, Y. Wang, Y. Xie, Y. Liang, A. Lin, and X. Wang, "The dual-current control strategy of grid-connected inverter with LCL filter," *IEEE Trans. Power Electron.*, vol. 34, no. 6, pp. 5940–5952, Jun. 2019.
[27] C. Xie, K. Li, J. Zou, D. Liu, and J. M. Guerrero, "Passivity-based design of grid-side current-controlled LCL-type grid-connected inverters," *IEEE Trans. Power Electron.*, vol. 35, no. 9, pp. 9813–9823, Sep. 2020.
[28] J. Sun, "Impedance-based stability criterion for grid-connected inverters," *IEEE Trans. Power Electron.*, vol. 26, no. 11, pp. 3075–3078, Nov. 2011.
[29] C. Zhang, X. Li, X. Xing, B. Zhang, R. Zhang, and B. Duan, "Modeling and mitigation of resonance current for modified LCL-type parallel inverters with inverter-side current control," *IEEE Trans. Ind. Informat.*, vol. 18, no. 2, pp. 932–942, Feb. 2022.
[30] Z. Chu, C. Qin, and X. Li, "Common-mode resonance current suppression method for the transformerless reduced switch count three-level inverter with LCCL filter," in *Proc. China Automat. Congr.*, 2023, pp. 9253–9257.
[31] Z. Lin, H. Zhang, P. Zhang, and Y. Li, "Analysis and reduction of zero-sequence LC-resonant current in DPWM-modulated 3φ LCL-type grid-connected inverter with neutral line," *IEEE Trans. Ind. Electron.*, vol. 71, no. 9, pp. 11721–11725, Sep. 2024.
[32] Z. Hu, X. Xing, C. Liu, R. Zhang, and F. Blaabjerg, "A modified discontinuous PWM method for three-level inverters with the improved LCL filter," *IEEE Trans. Power Electron*, vol. 39, no. 5, pp. 5498–5509, May 2024.
[33] A. Akhavan, H. R. Mohammadi, J. C. Vasquez, and J. M. Guerrero, "Passivity-based design of plug-and-play current-controlled grid-connected inverters," *IEEE Trans. Power Electron.*, vol. 35, no. 2, pp. 2135–2150, Feb. 2020.
[34] S. Li and H. Lin, "Passivity enhancement-based general design of capacitor current active damping for LCL-type grid-tied inverter," *IEEE Trans. Power Electron.*, vol. 38, no. 7, pp. 8223–8236, Jul. 2023,.
[35] X. Wang, Y. He, D. Pan, H. Zhang, Y. Ma, and X. Ruan, "Passivity enhancement for LCL-filtered inverter with grid current control and capacitor current active damping," *IEEE Trans. Power Electron.*, vol. 37, no. 4, pp. 3801–3812, Apr. 2022.

Rui Zhang (Member, IEEE) received the B.S. degree in electrical engineering from the Hefei University of Technology, Hefei, China, in 2019, and the Ph.D. degree in electrical engineering from Shandong University, Jinan, China, in 2025.

Since 2025, he has been a Postdoc with the School of Control Science and Engineering, Shandong University. His current research interests include control strategy of multilevel converters and power quality management.

Shumei Chi received the B.S. degree in electrical engineering from the Hefei University of Technology, Hefei, China, in 2019, and the M.S. degree in electrical engineering from Shanghai University of Electric Power, Shanghai, China, in 2022. She is currently working toward the Ph.D. degree in electrical engineering with Shandong University, Jinan, China.

Her current research interests include renewable power generation and power quality control.

Xiangyang Xing (Member, IEEE) was born in Rizhao, Shandong Province, China, in 1985. He received the B.S. degree in automation and the M.S. degree in control theory and application degree from Qufu Normal University, Qufu, China, in 2009 and 2012, respectively, and the Ph.D. degree in electrical engineering from Shandong University, Jinan, China, in 2016.

From 2017 to 2019, he was a Postdoctoral Research Fellow with Shandong University, Shandong, China. In 2019, he joined Shandong University, where he is currently an associate professor at the School of Control Science and Engineering.

His current research interests include multilevel converters, power conversion, and renewable power generation.

Chenghui Zhang (Fellow, IEEE) was born in Shandong, China, in 1963. He received the bachelor's and master's degrees in automation engineering from the Shandong University of Technology, Jinan, China, in 1985 and 1988, respectively, and the Ph.D. degree in control theory and operational research from Shandong University, Jinan, in 2001.

In 1988, he joined Shandong University, where he is currently a Professor with the School of Control Science and Engineering, the Chief Manager of Power Electronic Energy-saving Technology & Equipment Research Center of Education Ministry, a Specially Invited Cheung Kong Scholars Professor by China Ministry of Education, and a Taishan Scholar Special Adjunct Professor. He is also one of State-level candidates of "the New Century National Hundred, Thousand and Ten Thousand Talent Project", the Academic Leader of Innovation Team of Ministry of Education, and the Chief Expert of the National "863" high technological planning. His research interests include optimal control of engineering, power electronics and motor drives, energy-saving techniques, and time-delay systems.

Frede Blaabjerg (Fellow, IEEE) received the Ph.D. degree in electrical engineering at Aalborg University, Aalborg, Denmark, in 1995.

From 1987 to 1988, he was with ABB-Scandia, Randers, Denmark. He became an Assistant Professor in 1992, an Associate Professor in 1996, and a Full Professor of power electronics and drives in 1998 with AAU Energy, Aalborg. In 2017, he became a Villum Investigator. He is Honoris Causa with University Politehnica Timisoara (UPT), Timisoara, Romania, in 2017 and Tallinn Technical University (TTU), Tallinn, Estonia, in 2018. He has authored or coauthored more than 600 journal papers in the fields of power electronics and its applications, and he is the coauthor of four monographs and editor of ten books in power electronics and its applications. His current research interests include power electronics and its applications such as in wind turbines, PV systems, reliability, harmonics and adjustable speed drives.